Trajectory optimization for autonomous mobile robots in ITER

Alberto Vale[a], Daniel Fonte[b], Filipe Valente[a], Isabel Ribeiro[c]

[a]*Instituto de Plasmas e Fusão Nuclear, Instituto Superior Técnico, Universidade Técnica de Lisboa, Av. Rovisco Pais, 1049-001 Lisboa - Portugal*
[b]*Automotive Engineering, 1 Rue Galvani, Bâtiment C 91300, Massy - France*
[c]*Laboratório de Robótica e Sistemas em Engenharia e Ciência, Instituto Superior Técnico, Universidade Técnica de Lisboa, Av. Rovisco Pais, 1049-001 Lisboa - Portugal*

Abstract

The Cask and Plug Remote Handling System (CPRHS) is one of the remote handling systems that will operate in the International Thermonuclear Experimental Reactor (ITER), transporting heavy and highly activated in-vessel components between the Tokamak Building and the Hot Cell Building, the two main buildings of the nuclear facility. The CPRHS has similar dimensions as an autobus, maximum weight of 100 tons, with kinematics of a rhombic like vehicle (two drivable and steerable wheels) and has to move in cluttered environments. Two main approaches for trajectory optimization were developed and implemented aiming at providing smooth paths that maximize the clearance to obstacles taking into account the flexibility of rhombic like vehicles: line guidance (same path for both wheels) and free roaming (different paths for each wheel). The line guidance approach includes maneuvers when necessary and the ability of maximizing the common parts of different paths and used in the most of the nominal operations. Free roaming is mainly used when line guidance is not possible, namely in rescue operations. Both approaches were implemented in a standalone application that receives 2D CAD models of the buildings and returns the best trajectories, including a report of the most risky points of collision and the swept volume of the vehicle along the missions. This paper also presents the mains results of these approaches applied in the models of the real scenarios, crucial to proceed with the construction of the Tokamak Building. Conclusions and future work are presented and discussed.

Keywords: Path planning, Path optimization, Rhombic like vehicles, Line

1. Introduction

There is a practical need for developing and exploring nuclear fusion as a source of energy for the humankind benefit. The shortage predictions on fossil fuels, especially with the inevitable oil extraction decline, requires an urgent development and exploration of new sources of energy.

The current energy supply policy is mostly based on fossil fuels (oil, coal and natural gas) representing almost 80% of the total energy consumption, [21]. To worsen this scenario, the world population is expected to grow from 6 to 9 billion people until 2050, [30], resulting on an expressive raise of energy demand.

According to [20], no single technology is likely to provide all of the world's future energy needs and replace the actual oil-based energy infrastructure. It is important to achieve a more sustainable mix of fossil fuels but, more importantly, develop an energy consumption-frame based on new technologies and alternative energies such as solar, geothermal and nuclear, fission and fusion power.

The International Thermonuclear Experimental Reactor (ITER) project is a worldwide research experiment that aims to explore nuclear fusion as a viable source of energy for the coming years.

Besides the major scientific objective of exploring the nuclear fusion as a source of energy, future fusion power plants have to be safely and effectively maintained through Remote Handling (RH) techniques, due to restrictions on human being in activated areas.

Among the various RH systems that are expected to operate in ITER, as described in [22], this paper focus on a large and complex transporter unit that was chosen for the transfer of heavy and contaminated loads between the two main buildings of ITER, the Tokamak Building (TB), lodging the tokamak reactor and with access by vacuum vessel port cells (from this point forward simply identified as "ports") and the Hot Cell Building (HCB), that will work mainly as a support area. In Figure 1 it is depicted the two main buildings and their relative dimensions.

During ITER lifetime, the internal components of the vacuum vessel of the reactor, such as the blanket and divertor modules detached in Figure 1, will become activated due to exposure to highly energetic neutrons released

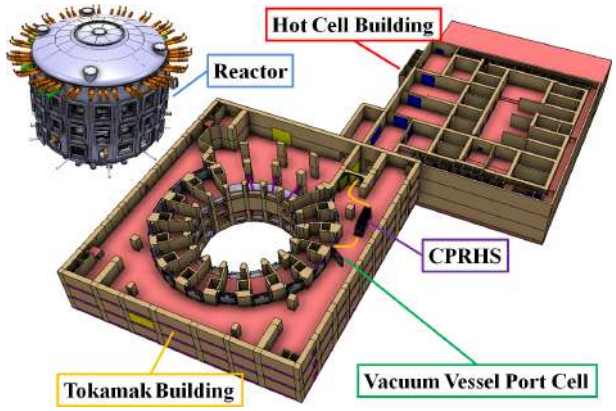

Figure 1: CAD models of the Tokamak Building, where the reactor is detached in the picture, the Hot Cell Building and the vehicle moving from the lift to a vacuum vessel port cell in level B1.

during the fusion reaction. Additionally, these in-vessel materials might get contaminated with small amounts of radioactive dust. Hence, the components that provide the base functions for the ITER machinery will need to be periodically inspected and upgraded. To manage such operations and provided that human presence will be not authorized in activated areas, the ITER maintenance system will mostly rely on RH devices.

The foreseen RH equipment will have a large impact on the design and assembly of the remaining ITER components, for instance, on building structural aspects and interfaces. Therefore, motion planning studies for the CPRHS in all its missions are required for the sake of the feasibility of the ITER structure design and the space reservation for the RH missions and to avoid the handwork to generate hundred of trajectories and also to speed up the study of the mission feasibility with the CPRHS.

The CPRHS, represented in Figure 2, is a large and complex transport unit to transport heavy and contaminated components between the TB and the HCB. The geometry of the CPRHS and its payload vary according to the cask and the components to be transported and hence, different CPRHS typologies will operate. As a reference, the largest CPRHS dimensions are 8.5m x 2.62m x 3.62m (length x width x height) and the total weight with the maximum load can reach up to 100 tons.

A CPRHS is composed by three sub-systems: the cask envelope (container that enclosures the in-vessel components and the RH tools to be transported),

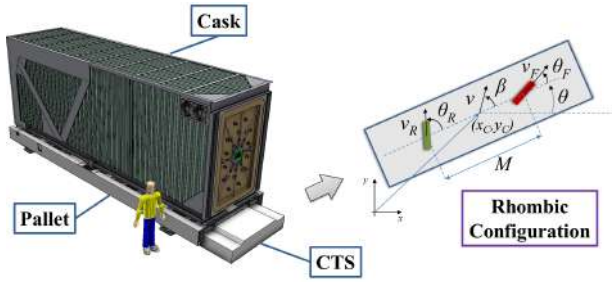

Figure 2: CAD model of the vehicle and the rhombic like configuration.

the Cask Transfer System (CTS), which acts as a mobile robot and the pallet (interface between the cask and the CTS equipped with an handling platform to support the cask load and help on docking procedures). When underneath the pallet the CTS transports the entire CPRHS, but it can also move independently of the pallet and cask. The CTS has a rhombic like configuration provided by two drivable and steerable wheels, identified as "F"ront and "R"ear wheels, as illustrated in Figure 2. Given this configuration, the CTS has a higher maneuverability in confined spaces than the traditional cars with Ackerman or tricycle configurations, [Dudek:10].

The CTS when operating individually or the CPRHS when carried out by the CTS are, hence, rhombic like vehicles. For a question of simplicity and from this point forward the CPRHS and the CTS when moving alone are identified as "vehicle".

As illustrated in Figure 2, consider the state vector $q = [x_c\, y_c\, \theta]$ as a representation of the vehicle pose in the frame $\{\mathrm{I}\}$, with (x_c, y_c) the coordinates of the center of the vehicle and θ the orientation of the vehicle. Also, consider v as the longitudinal speed and β the controllable sideslip angle of the vehicle, both defined in $\{\mathrm{I}\}$. A kinematic model for a rhombic like vehicle in $\{\mathrm{I}\}$, that allows the simulation of the vehicle motion directly through the desired longitudinal speed v, instead of imposing an individual linear speed for each wheel, was introduced in [15] as:

$$\begin{bmatrix} \dot{x}_c \\ \dot{y}_c \\ \dot{\theta}_m \end{bmatrix} = \begin{bmatrix} \cos(\theta+\beta) \\ \sin(\theta+\beta) \\ \frac{\cos\beta\cdot[\tan\theta_F - \tan\theta_R]}{M} \end{bmatrix} \cdot v, \tag{1}$$

where

$$\beta = \arctan\left(\frac{v_F \cdot \sin\theta_F + v_R \cdot \sin\theta_R}{2 \cdot v_R \cdot \cos\theta_R}\right) \tag{2}$$

and

$$v = \frac{v_F \cdot \cos\theta_F + v_R \cdot \cos\theta_R}{2 \cdot \cos\beta}. \tag{3}$$

This modeling entails that the wheels of the vehicle roll without slipping, a constraint inherent to the nonholonomy of rhombic like vehicles, and also considers a rigid body constraint, common to this type of vehicles, as follows:

$$v_F \cos\theta_F = v_R \cos\theta_R. \tag{4}$$

For the implementation, the $\dot{x}$ is considered as $(x(k+1) - x(k))/T$, where T is the sampling time and "k" the iteration. The (1), (2) and (3) become:

$$\begin{bmatrix} x_c(k+1) \\ y_c(k+1) \\ \theta_m(k+1) \end{bmatrix} = \begin{bmatrix} \cos(\theta(k) + \beta(k)) \\ \sin(\theta(k) + \beta(k)) \\ \frac{\cos\beta(k) \cdot [\tan\theta_F(k) - \tan\theta_R(k)]}{M} \end{bmatrix} \cdot v(k), \tag{5}$$

where

$$\beta(k) = \arctan\left(\frac{v_F(k) \cdot \sin\theta_F(k) + v_R(k) \cdot \sin\theta_R(k)}{2 \cdot v_R(k) \cdot \cos\theta_R(k)}\right) \tag{6}$$

and

$$v(k) = \frac{v_F(k) \cdot \cos\theta_F(k) + v_R(k) \cdot \cos\theta_R(k)}{2 \cdot \cos\beta(k)}. \tag{7}$$

The values $v_F(k)$, $v_R(k)$, $\theta_F(k)$ and $\theta_R(k)$ are the inputs. This implementation was inspired in the work described in [15] and detailed in [29].

A rhombic like vehicle has a particular capability, where both drivable and steerable wheels can follow the same path, as illustrated in the left image of Figure 3, which is identified as a line guidance approach. In general, each wheel can follow a different path keeping the structure of the vehicle, as illustrated in the right image of Figure 3, which is identified as free roaming approach. The relevance of these approaches will be addressed later in Section 2.

In ITER, the environment in all levels of TB and HCB is mostly composed by static and well structured scenarios. Therefore, each level of the buildings can be modeled using a 2D map representation. The adopted representation is a set of 2D points in a global cartesian referential of ITER and

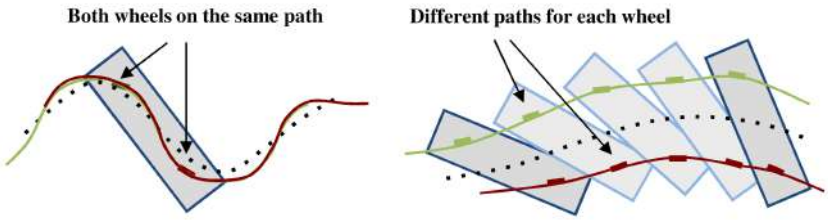

Figure 3: The drivable and steerable wheels of a rhombic like vehicle following the same path, feature identified as line guidance (left image) and following different paths, identified as free roaming (right image). The dotted lines represent the path described by the center of the vehicle.

a set of line segments, where each line segment connects two different points, as illustrated in the bottom images of Figure 4. It is assumed no crossing between lines. In case of intersection, a 2D point resulted from the intersection is created and each crossed line segment is split in two new line segments, one starting and the other ending in the splitting point, respectively.

The main challenge is to compute a trajectory to guide the vehicle from an initial vehicle configuration, q_S, to a final configuration, q_F, using the map representation and the vehicle model described above.

1.1. Paper Organization

The paper is organized as follows. The Section 1.2 summarizes the environment and its representation and describes the problem of trajectory optimization. The Section 2 describes the two main approaches for trajectory optimization, namely the line guidance and free roaming, including the features of maneuvers and the maximization of common parts of different trajectories. The Section 3 starts with a brief description of the software tool developed with the implementation of the algorithms and then presents the main results gathered within the scenarios of ITER. Finally, the Section 4 summarize the main conclusions and points for future work.

1.2. Problem Statement

The trajectory optimization problem stated for the vehicle consists on evaluating a trajectory, i.e., a geometric path combined with a speed profile, which guarantees that the vehicle, departing from an initial configuration, achieves the specified goal without colliding with obstacles and taking into account a safety margin. Specific optimization criteria such as smoothness,

path length and obstacle clearance are also considered during the planning phase as well as the vehicle characteristics (dimensions and kinematic constraints) and surrounding scenario.

To solve the trajectory optimization problem associated with the different missions specific information is required, which defines the inputs to the mentioned problem, as shown in Figure 4:

1. Vehicle model: the planning solutions depend directly on the vehicle configuration (geometric, kinematic and dynamic).
2. Environment model: the model of the scenario where the vehicles have to move that constitute relevant information for the definition of a collision free optimal planned solution. From the original CAD models in 3D, it is only used their 2D projection at floor level.
3. Initial and goal conditions: the pair of vehicle pose (position and orientation relative to a given referential) determining how the vehicles starts and finishes its motion.
4. Global trajectory(ies): most of the trajectories in TB share a large common path around the Tokamak, which is identified as a "ring" in each level. The maximization of different paths are also addressed, mainly in the TB to maximize the individual paths for each port in each level with the ring. Therefore, the trajectory of the ring is assumed also as an input.

Together, these inputs define a motion query for the specified mission in the ITER scenarios and are fed into a trajectory planner. This planner generates a path to be carried out by the vehicles, i.e., a set of cartesian coordinates (for specific vehicle reference points) and respective orientations that geometrically describe the vehicle motion. In addition to the geometric feasibility of the solution, which shall guarantee that the vehicle reaches the goal configuration without colliding with obstacles, and considering the particular characteristics of the transportation problem inside the ITER buildings, it is desirable that the planned solution follows specific criteria requirements:

- Path clearance: increase the minimum distance of the vehicle to the surrounding obstacles of the scenario.
- Path smoothness: the planned solution shall be smooth, minimizing steering maneuvers and jerky motions.

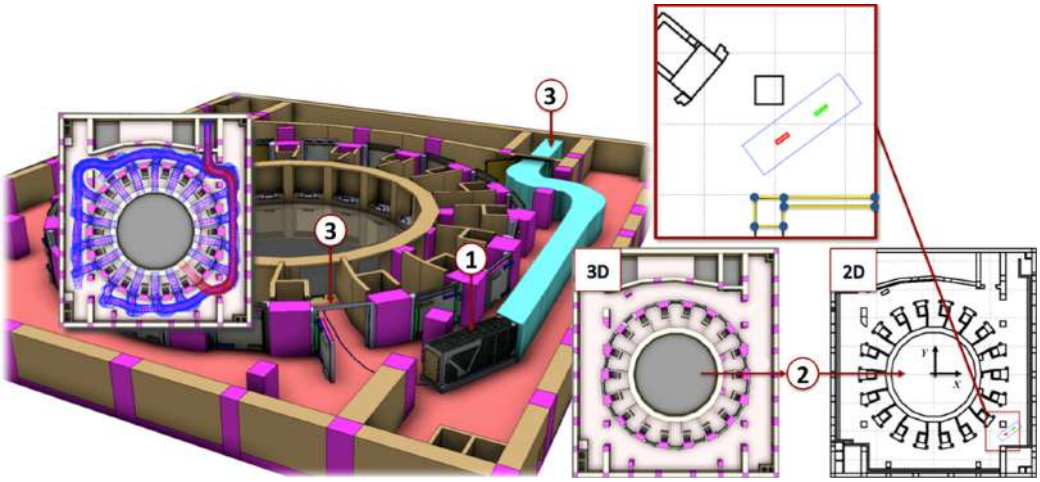

Figure 4: The main elements for the problem statement: the vehicle (1), the environment model (2) and the initial and final poses (3).

- Path length: whenever possible find the shortest possible solution, so as to minimize the energy consumption of the on-board batteries.
- Maximization of common paths: the vehicle journeys may share common paths through the buildings.

The planner shall output a trajectory, therefore the geometric solution (a path) is combined with a speed profile, which defines how to move the vehicle along the path at various speeds while satisfying the kinematic and dynamic constraints (maximum/minimum velocities and accelerations).

2. Path Planning and Trajectory Optimization

Two main approaches are presented for solving the trajectory optimization problem of rhombic like vehicles: the line guidance and the free roaming. The line guidance approach, where both drivable and steerable wheels follow the same path, is used in most of the trajectories. The line guidance approach, detailed in subsection 2.1, outputs an optimized trajectory without stops and without changing the motion direction. In some situations, the resulted trajectory from line guidance is not feasible in the entrances to some ports or to the lift, which may become feasible if including maneuvers. Therefore, an improvement of the line guidance approach using maneuvers is

described in subsection 2.2. When he trajectory is not feasible even if using maneuvers, the free roaming approach, detailed in subsection 2.3, is the last solution. The subsection 2.4 describes the speed evaluator adopted for both approaches, which converts the optimized paths into optimized trajectories. In addition, and in particular for the ITER scenario, specially in the TB, most of the trajectories share a long common part, since all the mission are between a different port of Tokamak and the single lift in TB. Therefore, an additional feature was developed for maximizing the common part of different trajectories, which is detailed in subsection 2.5.

The two main approaches, the line guidance and the free roaming, share three stages:

1. Geometric path evaluation: given the environment model and the initial and goal objectives, an initial geometric path is found. At this point the aim is to find a path connecting the initial and goal objectives that can act as an initial condition for the next path optimization stage.
2. Path optimization: this module receives the preceding geometric solution as input and returns an optimized path. The optimization process first applies a spline interpolation to satisfy weaker differential constraints such as smoothness requirements. Afterwards, a clearance based optimization is carried out to guarantee a collision free path that meets the safety requirements. In this study, a minimum safety distance between the vehicle and the obstacles must be guaranteed.
3. Trajectory evaluation: in this final module (described in subsection 2.4), a velocity function is defined along the optimized path transforming it into a trajectory, which is the output of the proposed planning approach.

The two first stages correspond to the path planning and optimization, while the third stage consists on the trajectory evaluation, including a velocity profile to the path. The two first stages are detailed in the sequel both for the line guidance and for the free roaming.

2.1. Line guidance

From previous work of RH in ITER [10] and for safety purposes the optimized paths would be implemented on the scenario using buried wired systems. In this navigation methodology, the vehicles would follow the path by using a line guidance approach, both wheels following the same path.

Given this ITER project requirement, the proposed planning methodology returns directly the path to be followed by the center of the wheels and not the one corresponding to the center of the vehicle.

A nominal operation of the vehicle for a specified environment determines a motion between two configurations (2D points with specific orientations). The first step of this planning methodology is to find an initial geometric path, i.e., a set of 2D points, connecting the initial and final configurations.

The geometric path must be optimized in terms of obstacle clearance and smoothness. The length is not a key issue, given the cluttered conditions of the scenario in ITER buildings, which constrains the set of possible paths. Instead of solving the problem of finding a path, as the work described in [18] and [19] based on Genetic Algorithms (GA), the main goal here is to have a deterministic approach to optimize the path in terms of obstacle clearance and smoothness, disregarding the length of the path. When a geometric path is not found, the inclusion of maneuver must be considered, which is a key issue in nonholonomic vehicles as described in [26] and described later in Section 2.2. However, the authors in [26] used the Rapidly-Exploring Random Tree (RRT), which is still a non deterministic approach and may become heavy for the line guidance. When non feasible path is found by the line guidance, the RRT is used in the free roaming approach, as described later in Section 2.3.

The environment in all levels of TB is composed by static and well structured scenarios. Therefore, the environments can be modeled using a planar map representation, ensuring good geometric properties, like low dimensionality and convexity. This encouraged the use of a combinatorial planning approach, over other approaches [9] and [11]. To handle this first planning objective, the use of a cell decomposition approach is considered, but other combinatorial approaches [3] and [4] could be used. From the existent cell decomposition approaches, a triangle cell arrangement was adopted, using the Constrained Delaunay Triangulation (CDT) [5], as illustrated on the left of Figure 5.

The overall procedure to determine an initial geometric path can be described as follows:

1. For a specified scenario, the CDT is applied to the corresponding 2D map yielding the triangle cell decomposition. Let C denote the set of N triangle cells so obtained, $C = \{C_n | n = 1, ..., N\}$. Since each triangle has three edges, only some of them may correspond to a wall

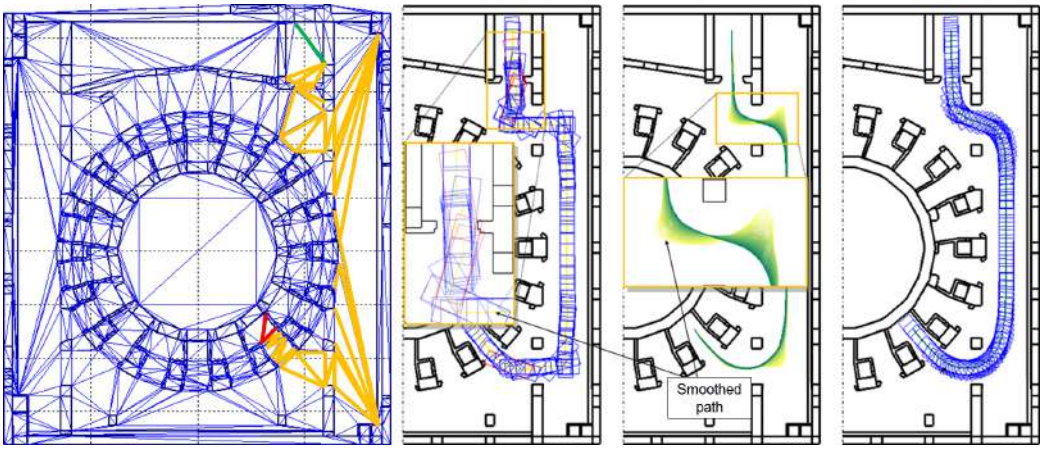

Figure 5: Example of line guidance approach applied in the trajectory evaluation to port 16 in level B1 of TB (from left to right: the initial map with the Constrained Delaunay Triangulation, the geometrical path, the evaluation of the optimization procedure and the final trajectory).

of the scenario and, then, identified as a real edge. The other edges, possible all of them, are identified as virtual edges since they exist only for computational purposes;

2. To handle a specific motion query, i.e., to connect an initial vehicle configuration, q_S, to a final configuration, q_F, the next step determines which cells, herein denoted by C_I and C_F, contain these two configurations;
3. Using the cell adjacency property, all the possible triangle sequences connecting C_I to C_F and composed by consecutive cells that do not share a real edge are evaluated. The desired cells in the sequences are connected by virtual edges, since feasible solutions cannot cross walls represented by real edges. Let $S = \{S_i | i = 1, ..., K\}$ be the set of all cell sequences. If such a sequence does not exist, the algorithm states that there is no solution for the proposed query;
4. Each cell sequence S_i is converted into an ordered sequence of points connected by line segments that can be interpreted as a graph. First, q_S is connected to the middle edge point of the first cell in each sequence. Then, the middle edge points of two consecutive cells of the sequence are taken as path sample points and are linked by a straight line. The middle edge point of the last cell in each sequence is connected to q_F;

5. This geometric solution is just a a sequence of few points. Then it is applied a spline interpolation to increase the number of points and, hence, to increase the resolution of the path.

The geometric path evaluation module just presented outputs all the possible geometric paths connecting q_S to q_F and composed by a set of line segments. To determine the best solution, the shortest path is chosen. To increase the efficiency of the CDT algorithm, the A^* algorithm, [2], is used in alternative to an exhaustive search. Simulations experiments shown how this algorithm can dramatically fasten the search for the shortest triangle cell sequence in complex scenarios such as the TB, that are composed off numerous triangle cells.

An optimization methodology was implemented, based on the elastic bands method [7]. The original concept associated with this approach appeared in the computer vision field, with the presentation of the so called "snakes" algorithm [6]. A snake is a deformable curve guided by artificial forces that pull it towards image features such as lines and edges. The solution herein proposed with the elastic bands methodology is similar to the snakes approach. Instead of retracting a curve to image features, in the path planning problem, it repels the path out from obstacles. Following this approach, the path is modeled as an elastic band which can be compared to a series of connected springs subjected to two types of forces:

- Internal forces: the internal contraction force simulates the Hooke's elasticity concept [8] and [16], i.e., the magnitude force is proportional to the amplitude of displacement. This modeling approach allows the simulation of the behavior of a stretched band. This is the reason why the paths become retracted and shorter. From this point on, it is adopted the term "elastic force", F_e, to refer to this force component;

- External forces: the obstacle clearance is achieved using repulsive forces, to keep the path, and consequently the vehicle, away from obstacles.

When submitted to these artificial forces, the elastic band is deformed over time becoming a shorter and smoother path, increasing clearance from obstacles. Hooke's law, evaluates the elastic force F_e applied to path point P_i in 8,

$$F_e(P_i) = k_e \cdot [(P_{i-1} - P_i) - (P_i - P_{i+1})] \tag{8}$$

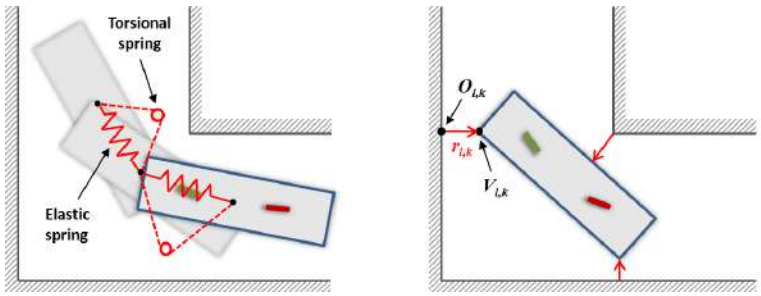

Figure 6: Elastic band concept: elastic forces to smooth the path (left image) and repulsive forces generated by the closest obstacles (right image).

where k_e is the elastic gain and P_{i-1} and P_{i+1} are the path points adjacent to P_i. The elastic band behavior can be controlled through k_e. The band stretches with high values of k_e while low values increase the band flexibility.

Using a collision detector algorithm, the nearest obstacle point (OP) to each vehicle pose might be considered. The use of a single OP as a reference to determine the repulsive forces may not be satisfactory to maintain clearance from obstacles, and therefore, a larger set of obstacle points, such as the k-nearest (k-OPs), must be considered, as illustrated in Figure 6. This will lead to a more balanced repulsive contribution ensuring effectiveness on most situations. Henceforth, on this formulation, it is considered the set of references formed by the nearest OP to each of the four vehicle's faces.

In the collision detector algorithm four situations may occur with the nearest points between the vehicle and the scenario: between a corner of the vehicle and a corner of the scenario, between a corner of the vehicle and a wall, between a corner of the scenario and a face of the vehicle and between a face of the vehicle and a wall (the vehicle is in parallel to a wall). In the three first situations, the result is always a point of the vehicle and point in the scenario, defining, as described later, in a distance and a direction for the repulsive force. In the last situation, when the vehicle is in parallel to a wall, an infinite number of points would be expected. However, any wall or any face of vehicle are line segments. Therefore, when this situation is verified, it is considered the closest points in the boundaries of the line segments.

The overall procedure to evaluate the repulsive force for each path point P_i is the following:

1. The initial poses (position and orientation) are determined based on

the constraint of both wheels placed over the path. The positions of both wheels cannot be exactly over a point of the ones that defines the path. Hence, it is necessary to estimate the poses of the vehicle in such a way that both wheels are over the path. The poses are estimated assuming that the vehicle follows the path in forward and backward direction:

- Forward direction: the rear wheel is fixed on each P_i. Next, it is necessary to find the closest point to the front wheel, i.e., the point P_j, such that

$$\|P_i - P_j\| \leq M \tag{9}$$

  where M defines the distance between front and rear wheels. The points P_i and P_j define the CPRHS/CTS pose. When the vehicle is close to the end of the path, it may not be possible to find a P_j and the algorithms jumps to the next step: backward direction.

- Backward direction: the same procedure is repeated, now fixing the front wheel for each P_i, as if the vehicle was executing the path moving backwards.

Let $k = \{1, ..., K\}$ denote the index of the k_{th} OP considered on each P_i related pose and $l = \{F, B\}$ referring to the forward or backward way. The $t_{l,k}$ is the vector defined by the k obstacle point ($O_{l,k}$) and each wheel point (W_F = rear wheel and W_B = front wheel),

$$t_{l,k} = W_l - O_{l,k} \tag{10}$$

This vector defines the repulsive force direction taking into account the position of the wheels. To maintain clearance from obstacles, the force magnitude must vary inversely with the distance of the poses to the obstacles. To carry out this geometric consideration, let $u_{l,k}$ denote the vector taken from the $O_{l,k}$ to the vehicle nearest point $V_{l,k}$,

$$u_{l,k} = V_{l,k} - O_{l,k} \tag{11}$$

2. Each pair of points ($O_{l,k}$,$V_{l,k}$) determines a repulsive contribution defined on P_i given by,

$$r_{l,k}(P_i) = \begin{cases} \frac{t_{l,k}}{\|t_{l,k}\|} f(\|u_{l,k}\|) & if\ \|u_{l,k}\| > d_{th} \\ \\ \frac{t_{l,k}}{\|t_{l,k}\|} f_{th} & if 0 \leq \|u_{l,k}\| \leq d_{th} \end{cases} \tag{12}$$

with f denoting a monotonically decreasing function, with a maximum reference value, f_{th}, to avoid outsized magnitude values when a threshold distance, d_{th}, is exceeded.

3. According to (12), the repulsive force for each P_i is determined as a combination of different repulsive contributions,

$$F_r(P_i) = k_r \cdot \sum_{l=\{F,B\}} \sum_{k=1}^{K} r_{l,k}(P_i) \tag{13}$$

with k_r denoting the repulsive gain.
Once the elastic (8) and the repulsive (13) forces are computed, an update equation procedure that defines the path evolution along each iteration is applied as

$$P_{i,new} = P_{i,old} + F_{total}(P_{i,old}) \tag{14}$$

with the total force contribution given by

$$F_{total}(P_{i,old}) = F_e(P_{i,old}) + F_r(P_{i,old}) \tag{15}$$

The stopping criteria is defined by detecting that magnitude changes on F_{total} are smaller than a given threshold or by setting a maximum number of iterations. The path optimization is thus carried out by a path deformation approach where the computed paths are treated as flexible and deformable bands. Elastic interactions smooth the path by removing any existing slack, whereas repulsive forces improve clearance from obstacles.

The Figure 7 illustrates the evaluation of the path optimization, showing the closest points of the scenario. At the end of the approach, running again the collision detector algorithm over the optimized path, identifies the closest points and how close they are. Hence, it is possible to identify the places of the scenario with high risk of clash, which is important for the feasibility analysis of the building design.

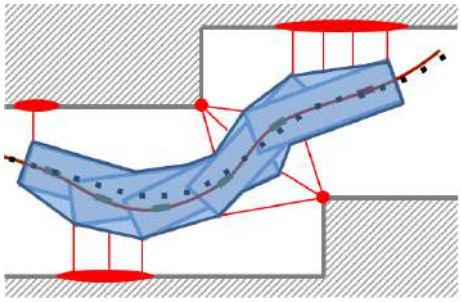

Figure 7: The most closest points between the scenario and the path evaluated by the line guidance.

2.2. Integration of maneuvers

There are particular situations where the described methodology of line guidance fails to generate feasible solutions, due to the confined environment. The integration of maneuvers can greatly improve the path planning, by providing a feasible solution where none could be found before and also by improving the distance to obstacles. The Figure 18 in the Section 3 illustrates an example in the vicinity of the lift, where the risk of collision is high if not consider maneuvers.

A maneuver exists when the vehicle stops and changes its motion direction, so as to achieve a specified orientation. In this paper, a maneuver splits the path in two sub-paths with the constraint that the final pose of the first sub-path is the initial pose of the next sub-path. In both sub-paths the line guidance methodology is considered.

By taking advantage of the vehicle kinematic configuration, the line guidance algorithm was improved to incorporate one or multiple maneuvers. In case n maneuvers are required, the path is divided in $n + 1$ sub-paths and the path optimization is applied to each sub-path. An additional constraint has to be taken into account when considering maneuvers. The path should be common to both wheels. However, when following a path, both wheels cannot follow the entire path. For instance, when following in forward direction, it is expected that the front wheel reaches the end of the path before the rear wheel. Similarly, in backwards direction, the rear wheel reaches the beginning of the path before the front wheel. This gap corresponds to the wheelbase, M. Consequently, this constraint should also be taken into consideration when evaluating maneuvers. Between two consecutive sub-paths

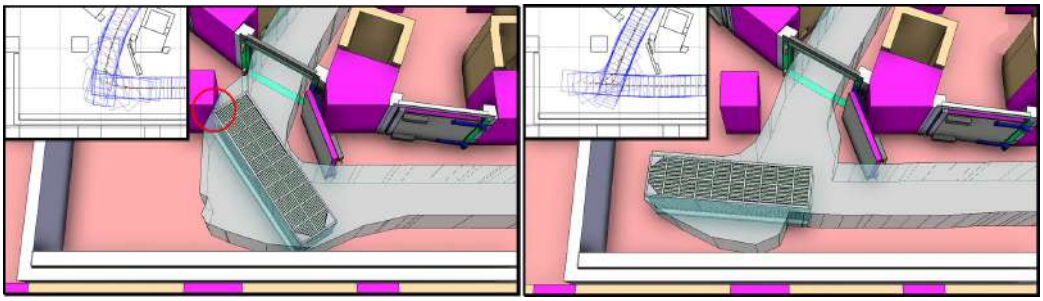

Figure 8: Trajectory to port 17 in level B1 of TB, without maneuver but with clash (left image) and feasible with a maneuver (right image).

of a maneuver, there is a coincident segment of both sub-paths with a length greater or equal to the distance between the wheels.

The decision of including maneuvers is taken when a path without maneuver is not feasible, as illustrated in Figure 8, where there is a collision, or does not fulfill the minimum safety distance to obstacles. The point(s) of maneuver are introduced manually. It is possible to choose if they are fixed or flexible. In this later case, the algorithm can adjust its position during the optimization to obtain the final trajectory.

2.3. Free roaming

The line guidance methodology entails that both vehicle wheels should follow the same physical path and therefore the inherent rhombic flexibility is only partially explored. Figure 9 illustrates part of the scenario in TB of ITER where a CPRHS, acting as a rescue vehicle, has to dock in a Vacuum Vessel Port Cell (VVPC) where another CPRHS is already parked. There is a possible trajectory for the first cask using line guidance, as illustrated in the first image of Figure 9. However, if considering the same constraint, the rescue vehicle clashes with the wall, as illustrated in the second image of Figure 9. In several situations as the previous one, no possible path is found for the second cask using the line guidance approach. In case of using independent references for the wheels, i.e., free roaming, a possible trajectory is found, as illustrated in the last image of Figure 9. This solution requires the use of dedicated motion planning techniques, in particular, the employment of an efficient path optimization method capable of handling the high maneuvering ability of the rhombic vehicle.

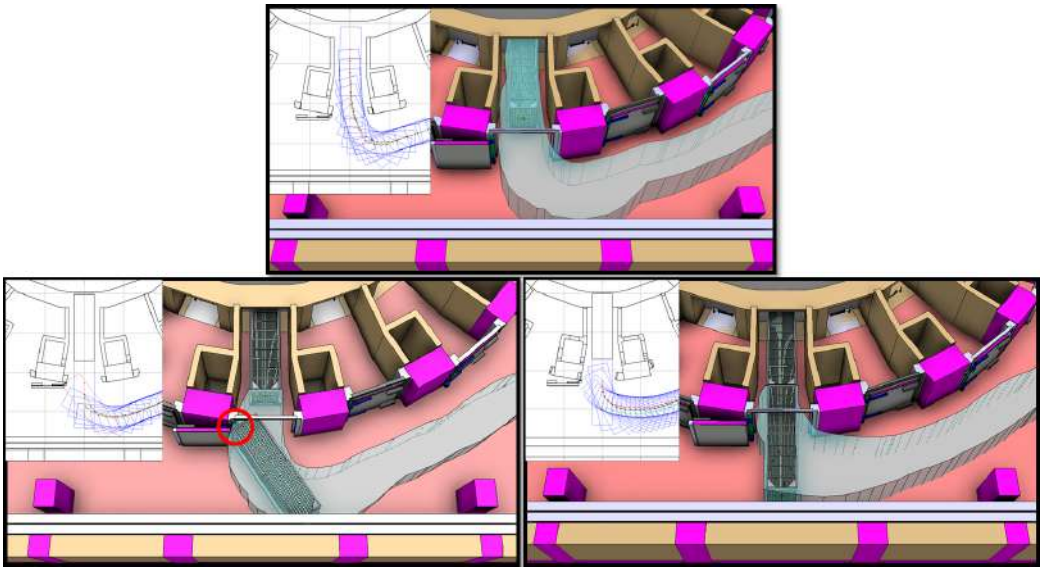

Figure 9: Trajectories for port 14 in any level of TB: (top image) the nominal operation is possible with line guidance, (bottom left image) in rescue operation, where a CPRHS is already docked, resulting in collision using the line guidance and (bottom right image) using free roaming results in a feasible trajectory.

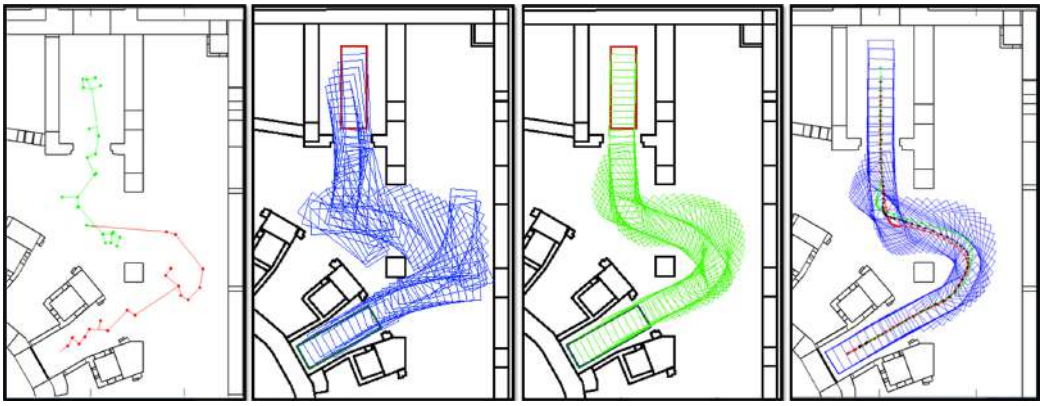

Figure 10: From left to right: the initial map, the Rapidly-Exploring Random Tree and the evaluation of free roaming.

The free roaming methodology acts on rough paths provided by global planners like the RRT, [14], or the Probabilistic Roadmap Method, (PRM) [9]. The proposed method redefines the elastic bands concept, [7], to evade the common approach that formulates paths as particle-systems. Inspired on the rigid body dynamics, consecutive poses along the rough path previously referred are treated as rigid bodies that are repelled from obstacles through external forces, improving path clearance. Additional interactions provide path connectivity and guarantee smooth transitions between vehicle poses. The bottom images of Figure 10 illustrate the free roaming process. This formulation allow to explicitly consider the vehicle geometry during the optimization and fully profit from the high maneuverability of rhombic vehicles.

In this approach, the use of rigid body dynamics is restricted to the case of *general plane motion*, i.e., the particles composing the rigid body move in parallel planes and their motion is neither characterized by pure rotational nor pure translational movements. Therefore, angular variables, such as moments and angular velocities, are scalar quantities.

Consider that a rigid body with a Center of Mass (CoM) denoted by C, is acted by N external forces, F_n, with $\{n = 1, \cdots, N\}$. Following the *Newton's Second Law* and taking the rigid body as a system of particles, the dynamics of C, with respect to the inertial frame OXY, is given by

$$F_{total} = \sum_{n=1}^{N} F_n = m \cdot a, \tag{16}$$

where m is the mass of the body and a is the linear acceleration of C. The dynamics of the rigid body motion relative to the its body frame, $CX'Y'$, is given by

$$\tau_{total} = \sum_{n=1}^{N} F_n \times e_n = I_C \alpha, \tag{17}$$

which entails that the resultant torque about C, τ_{total}, is a vector with the direction of the angular acceleration, α, and magnitude $I_C\alpha$. In (17), I_C is the moment of inertia around the perpendicular axis passing through C, whereas e_n corresponds to the position vector of F_n relative to the reference frame $CX'Y'$. For the case of uniformly accelerated motion, which will be adopted in this formulation, a and α assume constant values over time.

From the kinetics viewpoint, the general plane motion of the rigid body can be decomposed as the combination of a translation with linear acceleration, a, and a rotation about C with angular acceleration, α, given by (16) and (17), respectively. The linear, v, and angular, ω, velocities of the rigid body's CoM can be obtained through integration of a and α over time, t, as follows,

$$v = v^0 + at \tag{18}$$

$$\omega = \omega^0 + \alpha t \tag{19}$$

where v^0 and ω^0 are the initial linear and angular velocities.

The position, s, and orientation, θ, of the rigid body can be accessed through the integration of (18) and (19), yielding

$$s = s^0 + v^0 t + \frac{1}{2} a t^2 \tag{20}$$

$$\theta = \theta^0 + \omega^0 t + \frac{1}{2} \alpha t^2, \tag{21}$$

where s^0 and θ^0 are the initial position and orientation of the rigid body's CoM. Equations (16) - (21) completely describe the general plane motion of

a rigid body, relating displacement, velocity and acceleration to the external forces, which are the cause of motion.

The path optimization, based on a deformation process, refines and improves the quality of a rough solution path provided by a planner. This rough path, which defines the input for the optimization process, is consider to be a set of collision-free motions connecting the queried initial pose, q_S, and the final pose, q_F. From this time forward the rough path will be referred to as query path.

In the path optimization process, each of the consecutive vehicle poses that form the query path is treated as a rigid body that is connected with its adjacent poses like a convoy through internal interactions and subjected to external-repulsive forces produced by obstacles in its vicinity. Hence, the path optimization becomes a path deformation problem, which relies on the principles of rigid body dynamics to iteratively simulate the evolution of each pose on the optimization process. In particular, it is proposed to subject each vehicle pose in the query path to two types of efforts:

- Internal efforts: consecutive poses are kept connected through virtual elastic and torsional springs, which simulate the Hooke's elasticity concept and originate elastic forces and torsional torques. These efforts guarantee smoothness on deformation and help to shorten the path, and

- External efforts: repulsive forces repel the rigid poses from obstacles, acting as a collision avoidance feature. Moreover, force eccentricity originates repulsive rotating torques, which re-adapt poses orientation maximizing clearance over the obstacles.

Loosely following the *elastic bands* concept proposed by Quinlan and Khatib in [7], this method, by considering each vehicle pose as a rigid body, enables the path deformation to explicitly consider the vehicle geometry and exploits the rhombic vehicle nature, issues considered here as unattended on similar studies.

The implemented path optimization process based on elastic bands concept is described as follows. Let $j = \{1, \ldots, J\}$ be the index of the consecutive vehicle poses composing the query path, each defined by a configuration vector

$$q_j = \begin{bmatrix} s_j \\ \theta_j \end{bmatrix}, \tag{22}$$

where s_j and θ_j denote the position and the orientation of the pose q_j relative to a fixed reference frame, respectively. It is stated that $q_1 = q_S$ and $q_J = q_F$.

The elastic force, F_E, and the torsional torque, τ_T, evaluated for the vehicle pose at q_j are:

$$F_E(q_j) = K_E \cdot [(s_{j+1} - s_j) + (s_{j-1} - s_j)] \tag{23}$$

$$\tau_T(q_j) = K_T \cdot [(\theta_{j+1} - \theta_j) + (\theta_{j-1} - \theta_j)], \tag{24}$$

where K_E, the elasticity gain and, K_T, the torsional gain, control the elastic and torsional avoidance behavior on the path deformation, respectively.

The evaluation of the external efforts due to obstacle proximity relies on a heuristic-based collision detector module, which is capable of determining the set of i-nearest Obstacle Points (OPs) to each sampled pose q_j. The overall procedure to handle the evaluation of the repulsive forces and torques can be described as follows:

1. Let $i = \{1, \ldots, I\}$ denote the index of the *i-th* OP relative to a specific pose q_j. Let $u_{j,i}$ be the vector

$$u_{j,i} = V_{j,i} - O_{j,i}, \tag{25}$$

   taken from each OP, $O_{j,i}$, and the corresponding vehicle nearest point, $V_{j,i}$.

2. To improve clearance during path deformation, distance-dependent repulsive forces are defined, where each pair of points ($O_{j,i}$, $V_{j,i}$) determines a repulsive contribution. For a specific vehicle pose, q_j, the repulsive contributions are defined as

$$r_{j,i} = \frac{u_{j,i}}{\|u_{j,i}\|} \cdot f(\|u_{j,i}\|) \tag{26}$$

   where,

$$f(\|u_{j,i}\|) = \max(0, F_{max} - \frac{F_{max}}{d_{max}} \cdot \|u_{j,i}\|). \tag{27}$$

   In (27), a maximum allowable magnitude, F_{max}, is assigned to avoid outsized values in the close vicinity of the obstacles. d_{max} denotes the distance up to which the repulsive force is applied.

3. For each pose q_j, the total repulsive force is defined as

$$F_R(q_j) = \sum_{i=1}^{I} r_{j,i}. \tag{28}$$

Using (17), the net repulsive torque around the *j-th* pose CoM is defined as

$$\tau_R(q_j) = \sum_{i=1}^{I} r_{j,i} \times e_{j,i}. \tag{29}$$

The repulsive and elastic forces are combined on a total force contribution as,

$$F_{total}(q_j) = F_R(q_j) + F_E(q_j). \tag{30}$$

Similar approach is valid for the torsional and repulsive torques acting on each pose q_j. This leads to the definition of a net torque expressed as,

$$\tau_{total}(q_j) = \tau_T(q_j) + \tau_R(q_j). \tag{31}$$

Once determined the efforts acting on each pose, the ensued motion is evaluated through the principles of rigid body dynamics. Equations (16) and (17), are rewritten as

$$a_j = \frac{F_{total}(q_j)}{m} - K_D \cdot v_j \tag{32}$$

$$\alpha_j = \frac{\tau_{total}(q_j)}{I_C} - K_D \omega_j, \tag{33}$$

which provide the linear and angular accelerations for a specific pose q_j. The last term in the right hand side of (32) and (33) represent damping effects introduced to reduce the oscillatory motion during path deformation. They are controlled through K_D, herein set equally for both the translational and the rotational motion components. Notice that both m and I_C in (32)-(33), do not refer to real vehicle parameters but rather to simple scalars determining the resistance of each pose to change its configuration.

From a starting configuration in the query path, q_j, this pose is updated iteratively according to the set of equations (18)-(21), where the referred initial conditions are the previous iterated pose in this process. The stopping criteria is defined by setting a maximum number of iterations.

To solve the problem stated above the use of numerical integration methods is required. The simpler Euler integration method tends to be numerically unstable and less accurate for small rates [12], meaning that the path may oscillate widely and not reaching a stable configuration. In this approach it is proposed the use of the Leapfrog method, which is a modified version of the Verlet method [17] and is nicely discussed in [1]. The Leapfrog method is commonly used to integrate Newton's equations of motion offering a greater stability when compared to the simpler Euler method.

Assume that the time discretization interval is Δt and represent as $v_j^{k\Delta t} = v_j^k$ the value of the linear velocity of the pose iterated from q_j at time instant $k\Delta t$. The Leapfrog algorithm can be described for the previous stated approach as follows:

1. the linear, ${a_j}^k$, and the angular, α_j^k, accelerations are evaluated at a given time step k using (32) and (33) with v_j and ω_j given by (39) and (40) and F_{total} and τ_{total} evaluated at ${q_j}^k$;
2. the corresponding velocities are calculated for the next "half step" (i.e., $k + \frac{1}{2}$) as
$$v_j^{k+1/2} = v_j^{k-1/2} + \Delta t a_j^{k-1}, \tag{34}$$
$$\omega_j^{k+1/2} = \omega_j^{k-1/2} + \Delta t \alpha_j^{k-1}; \tag{35}$$
3. accordingly, the iterated configuration of the pose q_j at time instant $k+1$ is then updated from the iterated configuration of the pose at time instant k as
$$q_j^{k+1} = \begin{bmatrix} s_j^{k+1} \\ \\ \theta_j^{k+1} \end{bmatrix} = q_j^k + \Delta t \begin{bmatrix} v_j^{k+1/2} \\ \\ \omega_j^{k+1/2} \end{bmatrix} \tag{36}$$
for $k \geq 0$. Note that $q_j^0 = q_j$, the pose at the query path.

It remains an issue how to evaluate the velocity at the next half-step when only the starting conditions are given. To get the calculation started and, as suggested in [1], the following simple approximation is used
$$v_j^{1/2} = v_j^0 + \frac{\Delta t}{2} a_j^0 \tag{37}$$

$$\omega_j^{1/2} = \omega_j^0 + \frac{\Delta t}{2}\alpha_j^0. \tag{38}$$

The velocities at any given instant k are interpolated with

$$v_j^k = \frac{1}{2}[v_j^{k+1/2} + v_j^{k-1/2}] \tag{39}$$

$$\omega_j^k = \frac{1}{2}[\omega_j^{k+1/2} + \omega_j^{k-1/2}]. \tag{40}$$

The rigid body dynamics herein described is an approach for generate a trajectory. The dynamics of the vehicle are not addressed.

The line guidance and the free roaming approaches were described. Further results are presented in Section 3.

2.4. From path to trajectory

The output of the path optimization module of the planning methodology, using line guidance or free roaming, is a collision free path suitable for execution. To achieve a realistic plan, it is necessary to determine how the vehicle should move along the path satisfying dynamic constraints, i.e., the optimized paths should be parameterized in terms of velocities, converting the paths into trajectories. The definition of the vehicle's velocity along the path assumes a particular importance in this study. The designed trajectories must guarantee that the vehicle performs its motion in the shortest time period satisfying energy minimization. On the other hand, safety requirements are mandatory and the risk of collision shall be reduced. Given the cluttered environment where the CPRHS/CTS moves, an initial approach might define the vehicle speed profile as a function of the distance to the obstacles. The velocity assumes low values when the vehicle is closer to the obstacles. Otherwise, the velocity could be higher, under safety levels. To generate this initial speed profile, the minimum distance of each path point in the optimized path to the closest obstacles is identified, as shown in Figure 11 - left. Each sampled value of minimum distance refers to a specific path point, p_i, and is measured considering the positioning of the vehicle when in this point (front or rear wheel), as if following the optimized path (see Figure 11 - right).

From the evolution of the minimum distance to obstacles, also referred as clearance profile, it is possible to determine an initialization for the vehicle's

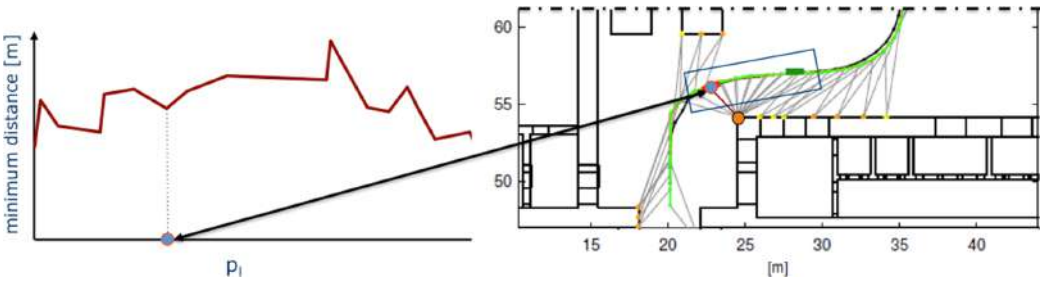

Figure 11: Evolution of the minimum distances to obstacles along an optimized path (left) and the respective path in the scenario, part of level B2 of HCB (right).

speed, which determines the speed at each reference point p_l, denoted as s_i, defined as a linear function of the minimum distance, d_i, included in the clearance profile as follows.

$$s_i = \begin{cases} s_{min} & if \quad d_i < d_{safe} \\ \alpha(d_i) & if \quad d_{safe} \leq d_i < d_{th} \\ s_{max} & if \quad d_i \geq d_{th} \end{cases} \tag{41}$$

A maximum and minimum allowable speed, s_{max} and s_{min}, are set to this profile, in order to integrate kinematic constraints. The safety margin is denoted as d_{safe} and d_{th} identifies the threshold distance above which s_{max} is considered. The speed profile thus obtained is saturated when d_i is above d_{th} or below d_{safe} and is referred as C-based speed profile, [28], as illustrated in Figure 12 - top left. However, the C-based speed profile is unable to handle vehicle dynamics constraints, meaning that the constraints on the admissible accelerations of the vehicle are ignored. To sidestep this issue, it was developed a specific routine, which tests each one of the C-based speed profile transitions, checking whether the accelerations are feasible or not. Whenever a dynamic unfeasible transition is found (e.g., the calculated acceleration is higher than the admissible maximum value a_{max} or lower than the admissible minimum value a_{min}), the routine corrects the speed accordingly. In Figure 12 - top right, the difference between the C-based profile (yellow) and re-evaluated speed profile based on vehicle dynamics (green) is depicted.

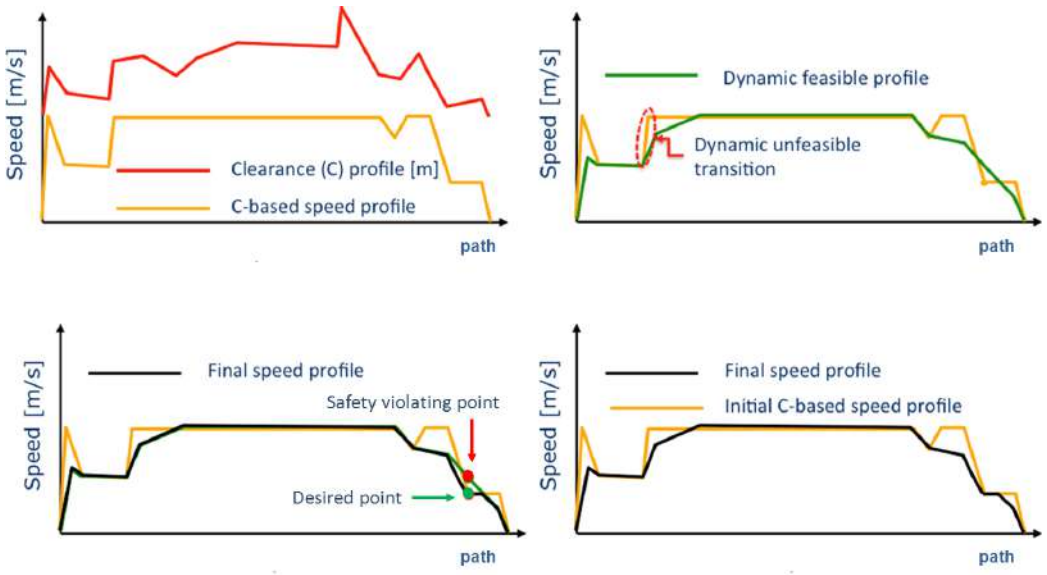

Figure 12: Flow diagram for the evaluation of a speed profile that is both compliant with safety (from the proximity with obstacles) and dynamic (from the vehicle) constraints.

The transition from a clearance based profile to a dynamic feasible profile may lead to a violation of the initial safety restrictions as it is signaled in Figure 12 - bottom left. This means that the evaluated speed profile may include values that are higher than those desired, given the obstacle proximity. When these transgressions are detected, the final profile is generated by considering both safety requirements and vehicle dynamics constraints as illustrated in the bottom right of Figure 12. The obtained speed profile can be significantly different from the initial C-based speed profile and when combined with the optimized path, the final optimized trajectory is obtained.

A typical optimized trajectory obtained is shown in Figure 13 along with the speed variation along the path ($a_{max} = 0.01m/s^2$, $d_{safe} = 0.3m$, $d_{th} = 1m$).

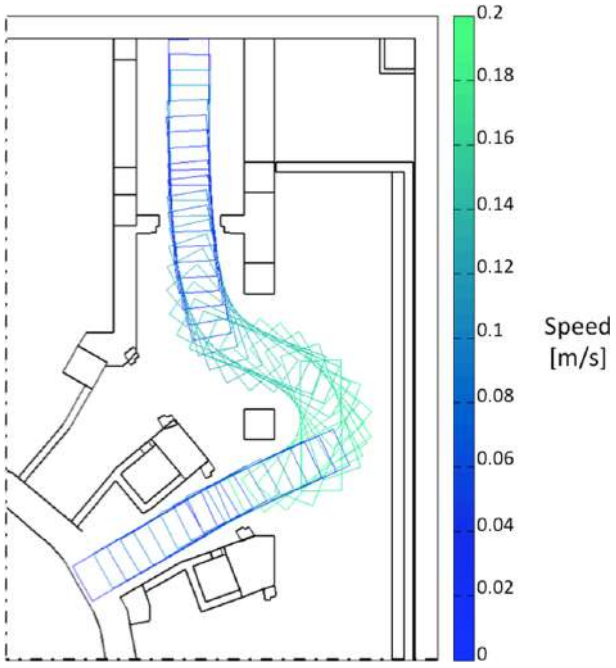

Figure 13: CPRHS speed map for a journey to port cell 2 in level L1 of TB.

2.5. Maximization of common parts

The geometry of the scenarios in TB and HCB is such that paths for different missions of the CPRHS can, in certain situations, share common parts. In particular, this is noticeable in the galleries around the tokamak where all CPRHS have to travel from/to the lift to/from each of the port cells. The maximization of common parts in different paths minimizes the overall volume required for CPRHS operation, this being a key issue in ITER design and safety. To achieve this goal, the line guidance approach described in Section 2.1 was improved with a feature for maximizing the common parts of different trajectories.

Around the galleries in TB an optimal path to be followed using line guidance navigation was generated (Figure 14 - left). It is to be used, as much as possible, in all missions from/to the lift to/from each port that are accessible from the gallery. For each path, two issues arise at this stage: i) where to deviate from this common part of the path to reach a particular port, and ii) which is the optimal path from this deviation point, to the final goal in the port cell. The last path, i.e., from the deviation point to the final

goal, can be optimized using line guidance or free roaming, since the entrance to the port cell is more critical, given the risk of clashes with the pillars.

The overall procedure to evaluate an optimized trajectory that considers the maximization of common paths is illustrated in Figure 14 and can be described as follows:

1. Assume as an input the path starting from the lift and describing a ring around the galleries. This path can be evaluated using the same algorithm of Section 2.1.
2. Obtain a second optimized path from the lift to a specific port. In case of a non feasible trajectory using the line guidance, the second path is evaluated using free roaming. Note that, along the ring, both paths are quite similar.
3. Starting from the end point of the second path (obtained in point 2) and crawling backwards, the most closest point between the two paths is searched and defined as the Closest Point (CP), as illustrated in Figure 14. From the CP and crawling backwards a constant factor in the first path is defined the Splitting Point (SP). The common path is defined between the initial point of both paths and the SP.
4. The path starting in the SP, where the pose of vehicle is frozen, and finishing in the target goal is optimized following the same procedure of line guidance described in Section 2.1 or, if it is not possible, using the free roaming described in Section 2.3 . This means that the path in point 2 is now disregarded. At this point it is guaranteed the continuity in the splitting point.

The resulted path is finally inputted to the speed evaluator, leading to an optimized trajectory.

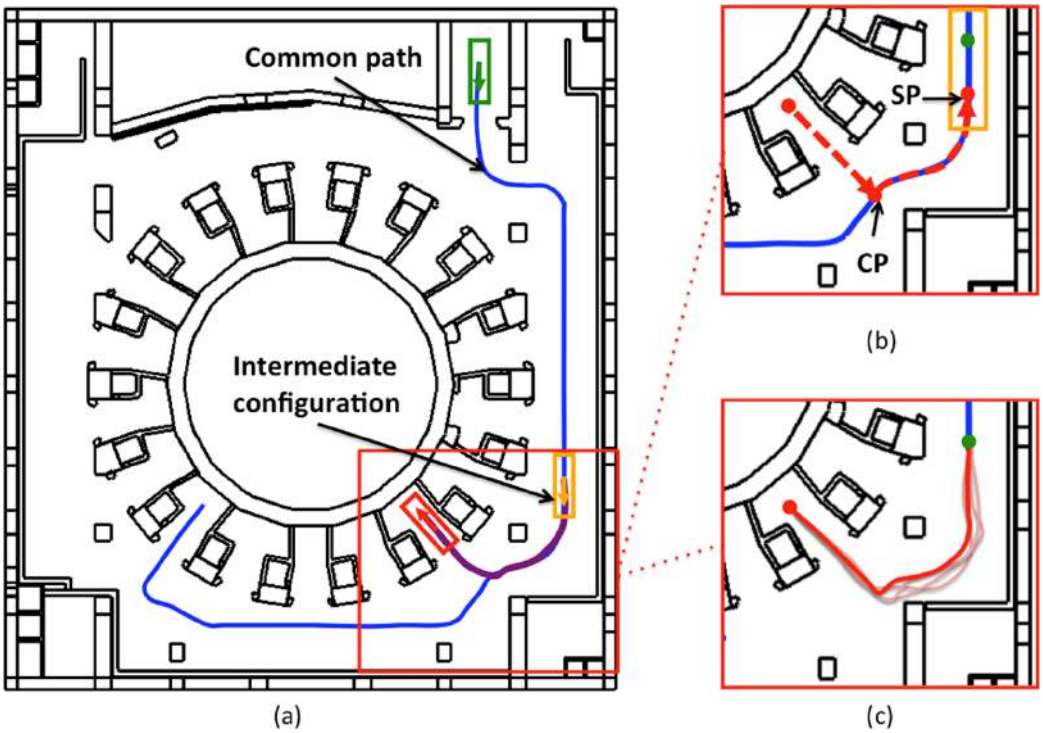

Figure 14: Example of the maximization of common parts: a) trajectories from the lift to ports 12 and 16 in level B1 of TB, b) the closest point, i.e., the point where the path to port 12 starts to be different and c) the evaluation of the path from the splitting point until the end.

3. Results

The algorithms were implemented in the specially designed software tool Trajectory Evaluator and Simulator (TES), developed under the grants F4E-GRT-016 and F4E-GRT-276-01, of the European Joint Undertaking for ITER and the Development of Fusion Energy. The TES was developed to generate trajectories using line guidance and free roaming approaches, for the evaluation of the 3D volume swept by the vehicle in CATIA V5R19 format and for the evaluation of common parts of different trajectories. The TES receives the models of the buildings and the models of different vehicles typologies and exports the optimized trajectories and the corresponding 3D swept volume directly to CATIA V5R19. The TES provides also a GUI to preview the trajectory optimization, to manipulate the scenarios (for instance to test

modifications in the port doors aperture configuration if necessary), to easily choose the vehicle typology to be used in the simulation and to generate results. Some snapshots of TES are presented in Figure 15, illustrating some features, including the exportation to CATIA V5R19. The output of TES is a set of optimized trajectories, which under the scope of the previously mentioned grants, were validated by an independent software developed by ASTRIUM SAS [27]. Additionally, TES provides trajectory information that will allow for the comparison of the different trajectory scenarios, i.e., both wheels following the same path or following different paths, the ability to evaluate the risk of a clash and the time duration for a journey.

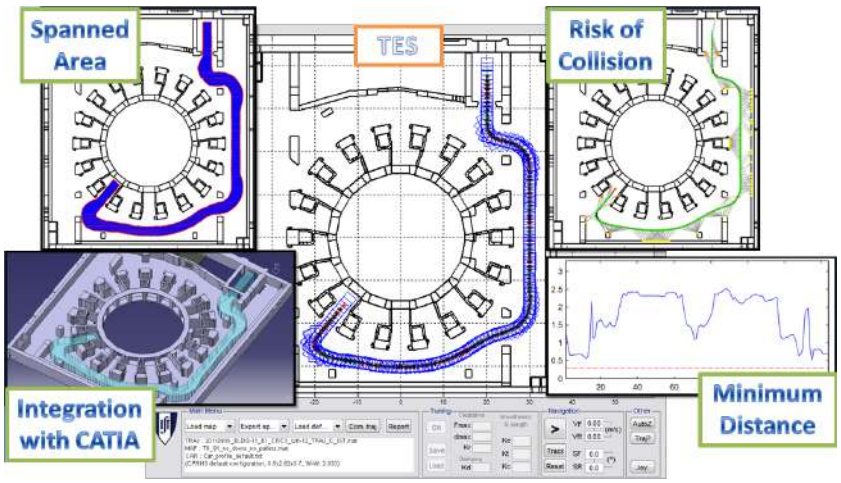

Figure 15: Snapshots of the Trajectory Evaluator and Simulator software application.

The simulated results were gathered using the maps of the three levels of TB and the four levels of HCB for trajectory optimization (including trajectories for nominal operation of transportation, rescue and for parking). Most of the trajectories are between the lift and a port in TB, and a docking port or a parking place in the HCB. Wherever possible, the line guidance approach is selected to find an optimized trajectory. The Figure 16 illustrates an optimized trajectory using line guidance between the lift and the port 2 of level B1 in TB. The Figure 16 - left illustrates the common path of both wheels, the paths described by the wheels and by the center of the vehicle and a sample of poses along the path. The Figure 16 - center represents the most critical points of the scenario associated to the path, i.e., the closest obstacles

to the vehicle when it crosses each point of the path. The danger level is coded by a gradient color, where red corresponds to the most dangerous situation. It is noticed that the critical points are most of the times the corners, in particular the entrances to the lift and to the ports. The third image represents the area swept by the vehicle when following the optimized path, i.e., the reserved area where no other elements are allowed aiming at avoiding collisions. Around the swept area it is also presented an extrusion of 30 cm that represents a safety margin; if an element is placed there, no collision is verified, but the risk of clash is high. In Figure 17 it is quantified the minimum distances to obstacles along the path and the speed profile for the trajectory presented in Figure 16.

Figure 16: Trajectory to port 2 using line guidance (from left to right), path and sampling poses, the most closest obstacles and the area spanned by the vehicle along the path.

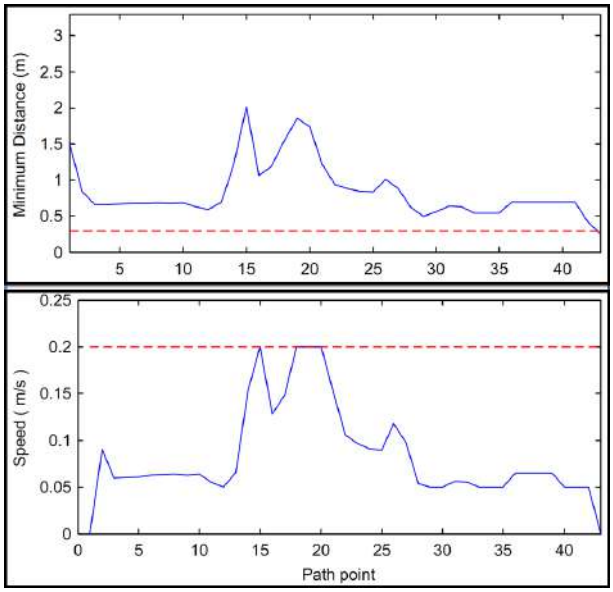

Figure 17: The minimum distance to the closest obstacles (top) and the respective speed profile (bottom) along the trajectory to port 2 in level B1 of TB using line guidance.

In some situations, the free space constrains the usage of the line guidance as illustrated in Figure 18 - left: the optimized path may not result in collision but the safety margin in the entrance to the lift is not fulfilled. Therefore, a maneuver is adopted, as illustrated in the right side of Figure 18. The minimum distances are greater in a trajectory with a maneuver, as illustrated in Figure 19, mainly between the points 6 and 12 of the trajectory. Each path is a set of points and the horizontal axis in Figure 19 represents the indexes of those points.

The Figure 20 illustrates the example of port 14, where line guidance can not provide a feasible trajectory, even if including maneuvers. The solution is to adopt the free roaming approach. Given the maximization of common parts of different trajectories, the free roaming is only adopted on the image of the Figure 20 in the vicinity of the entrance to the port, while the other part of the trajectory is accomplished using line guidance.

The line guidance is always adopted as the first choice for the trajectory optimization. However, all the feasible trajectories evaluated using the line guidance approach can also be evaluated or improved using the free roaming approach. The line guidance approach can be seen as a particular case of the

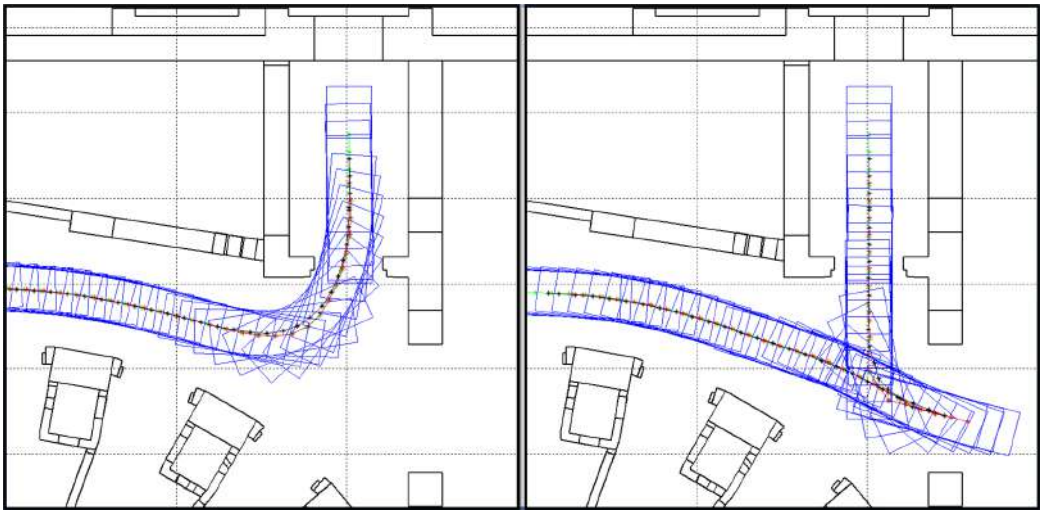

Figure 18: Optimized trajectory in the vicinity of the lift using line guidance without maneuver (left) and with a maneuver (right).

free roaming, i.e., when the paths of both wheels are coincident, it becomes the solution of the line guidance approach.

In terms of ITER requirements, if a trajectory evaluated using line guidance is feasible for a particular mission, the free roaming is not studied. Even though and for the purpose of this paper, shows in Figure 21 the comparison between the two approaches for port 1 in level B1 of TB, where both approaches are feasible. The trajectories are similar, but in the vicinity of the entrances to the lift and to the port, the differences between the paths of each wheel are more emphasized. In addition, the space swept by the cask when moving along a trajectory evaluated by the free roaming approach is larger when compared with the line guidance approach. In the example illustrated in Figure 21, the total swept area using line guidance is $173.3m^2$, while using the free roaming is $182.2m^2$, i.e., 5% more. However, the major difference is along the distances to the closest obstacles when the vehicle is moving along the paths. As illustrated in Figure 22, the free roaming provides a better safety distance when the vehicle is closer to the obstacles. In particular, in the entrance to the port (around the trajectory point 40), the minimum distance to the closest obstacle along the trajectory evaluated by the line guidance approach is closer to the safety margin, while the free roaming approach results in a trajectory with additional 15 cm of safety margin. It is

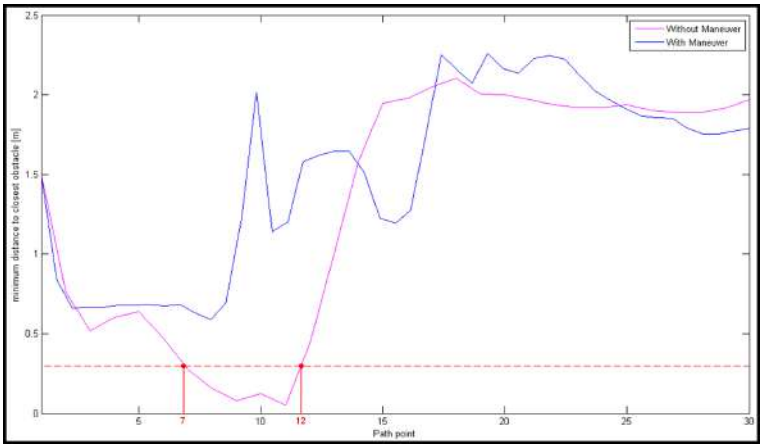

Figure 19: The minimum distance to the closest obstacles with and without the maneuver in the vicinity of the entrance to the lift.

a substantial value when the minimum safety margins allowed in ITER are between 10 cm and 30 cm.

The maximization of common parts from different trajectories is more noticeable for long trajectories, as in the examples illustrated in Figure 23 and Figure 24: trajectories for ports 12 and 13 in level B1 of TB. The Figure 23 illustrates the trajectories evaluated separately. The trajectories are quite similar, with the exception in the vicinity of the ports or closer to the pillars. The Figure 24 illustrates both trajectories to the same ports, but maximized with the common path around the tokamak. The main difference is visible outside the lift, since the common path around the tokamak took into consideration the other trajectories that are counter clockwise and requires maneuvers (see the example of Figure 8) and also the trajectory for port 2 (see the Figure 16). The resulted trajectory of maximization the common part seems to have less waypoints when compared with the trajectories that were evaluated individually. The number of points are equal, with the difference that the points are exactly the same for both trajectories maximized with the common part until the splitting point of the first trajectory (to the port 13). The minimum distances along the trajectories to port 12 and 13 obtained with and without the maximization of the common part are plotted in Figure 25 and Figure 26. The trajectories resulted from the maximization of common parts provide better results since they decrease the effect of the

Figure 20: Comparison of non feasible trajectory using line guidance (left image) and the feasible trajectory using free roaming (right image) to port 14 in level B1 of TB.

smoothness and increase the clearance. However, the minimum values, which corresponds to the entrance to the ports, remain approximately the same.

A total of 536 trajectories were optimized: 304 for the 4 levels in HCB and 233 for the 3 levels in TB, for different cask typologies and using the values presented in Table 1. The 3D CAD models of the occupied volumes were generated for all trajectories. The Figure 27 illustrates all the trajectories for the nominal operations and the respective occupied volume in level B1 of TB. The common path is similar to a ring around the tokamak. The Figure 28 illustrates all the trajectories for the nominal operations and the respective occupied volumes in level L1 of HCB. The common path is simply a straight line.

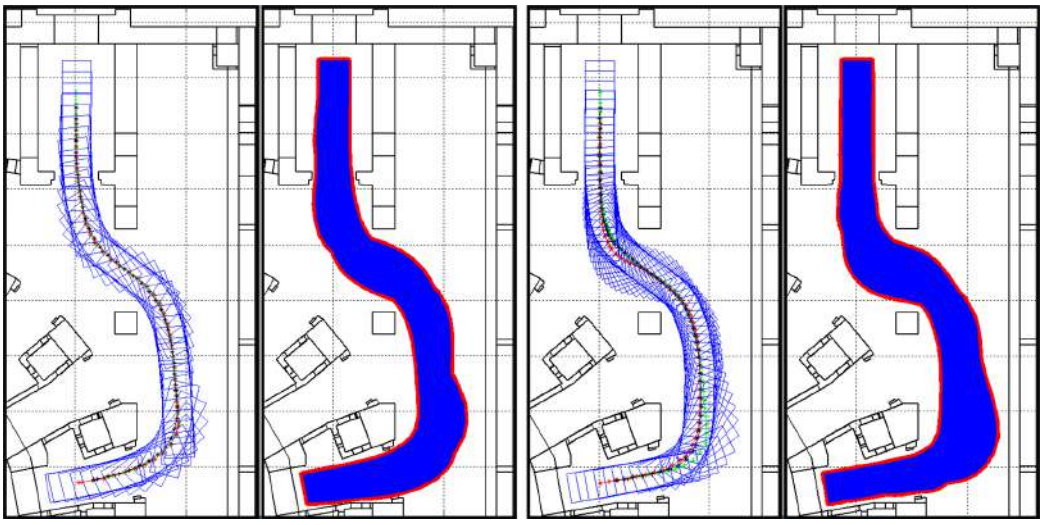

Figure 21: Trajectory to port 1 in level B1 of TB (from left to right: line guidance and the respective spanned area, free roaming and the respective spanned area.

Casks	Line Guidance				Free Roaming					
	K_e	K_r	F_{max}	d_{max}	K_c	K_e	K_d	K_t	F_{max}	d_{max}
CPRHS	0.3-0.4	0.05-0.1	1	1	0	1	2	300	1	1
CTS	0.3-0.5	0.05-0.1	1-1.5	0.5-2	0	1	2	300	1	1
Rescue	0.3-0.5	0.05-0.1	1-1.5	0.5-2	2	5	1	500	1	1
Parking	0.3-0.5	0.05-0.1	1-1.5	0.5-2	0	1	2	300	1	1

Table 1: Values used in the experimental results, where m and I_c were assumed as 0.5 and 3.29, respectively.

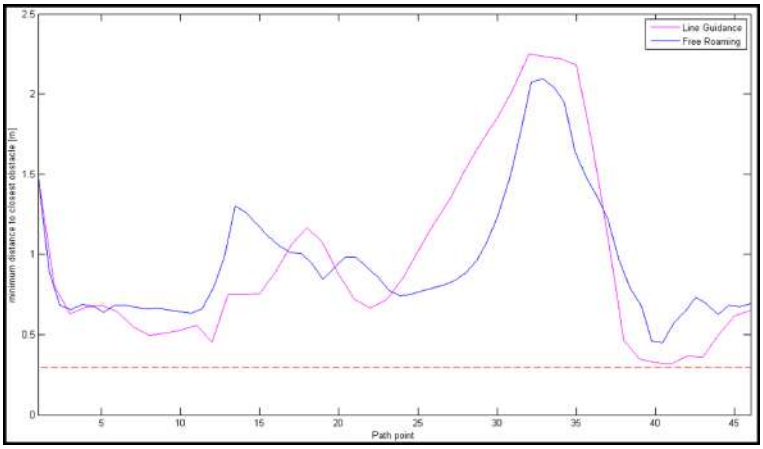

Figure 22: Comparison of minimum distance to the closest obstacles between line guidance and free roaming trajectories to pot 1 in level B1 of TB.

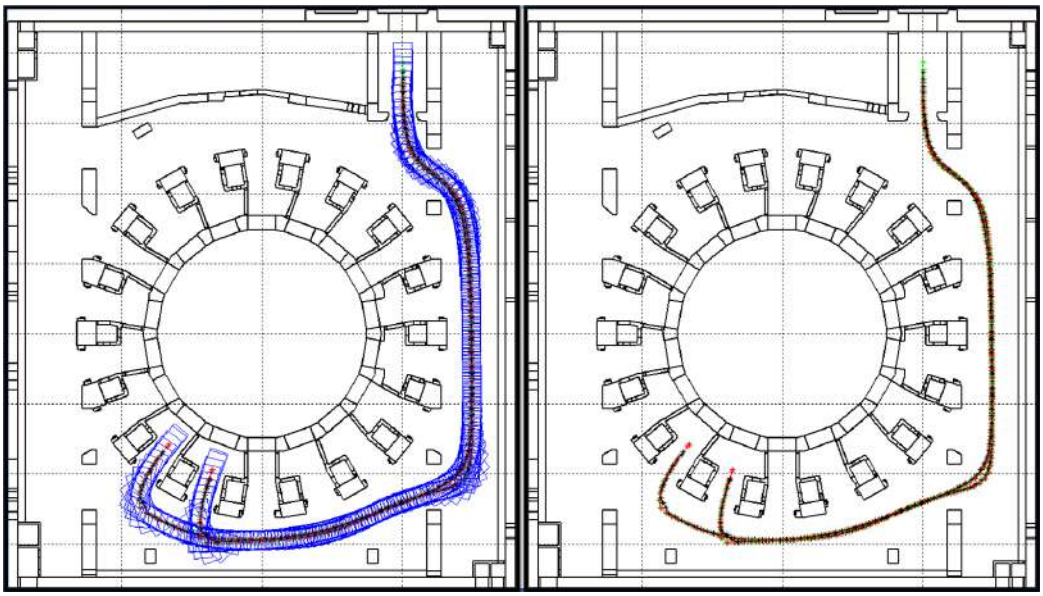

Figure 23: Trajectories to ports 12 and 13 in level B1 of TB using line guidance without maximization of common parts: sampling poses (left) and the waypoints (right).

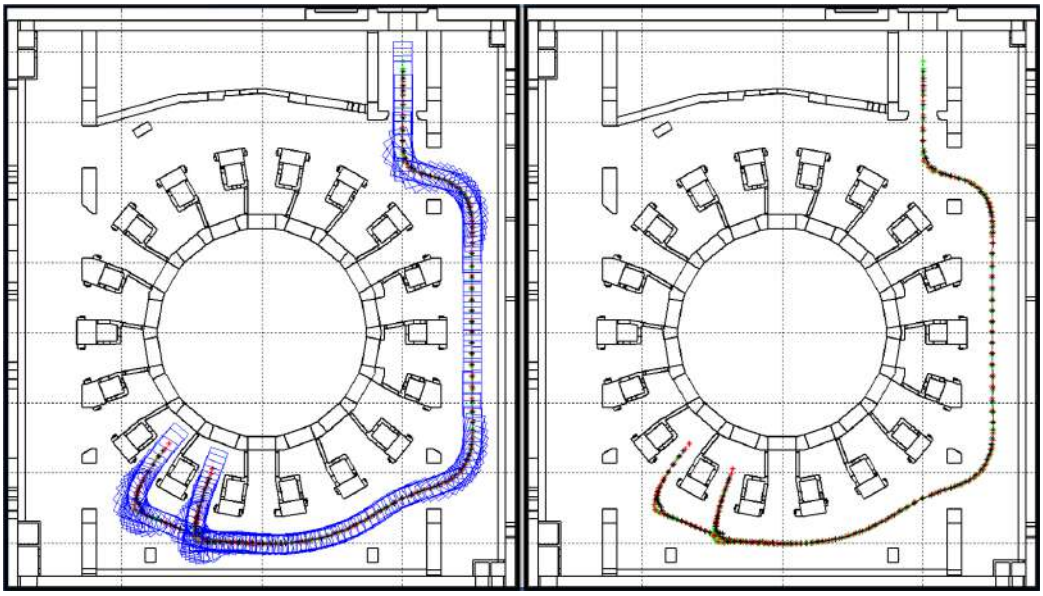

Figure 24: Trajectories to ports 12 and 13 in level B1 of TB using line guidance with maximization of common parts: sampling poses (left) and the waypoints (right).

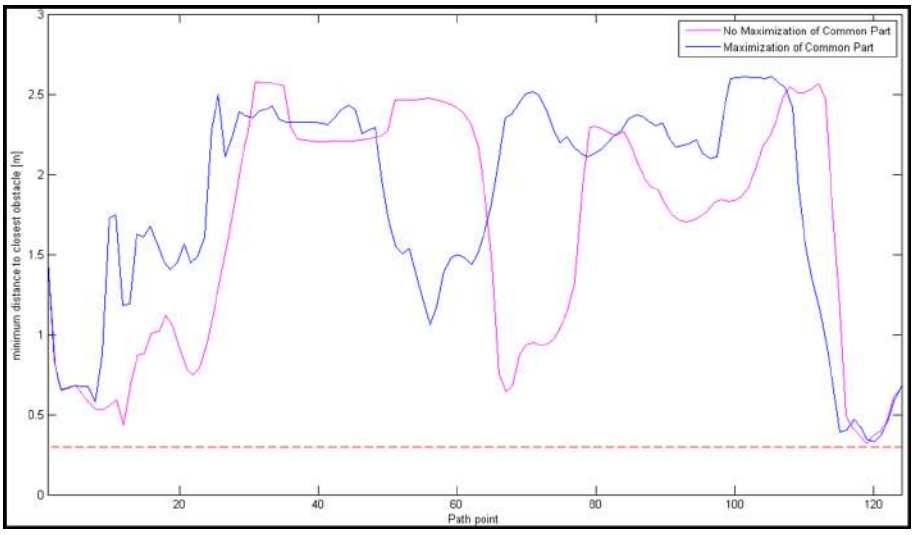

Figure 25: Comparison of the minimum distances to the closest obstacles using line guidance trajectories to port 12, with and without maximization of common part.

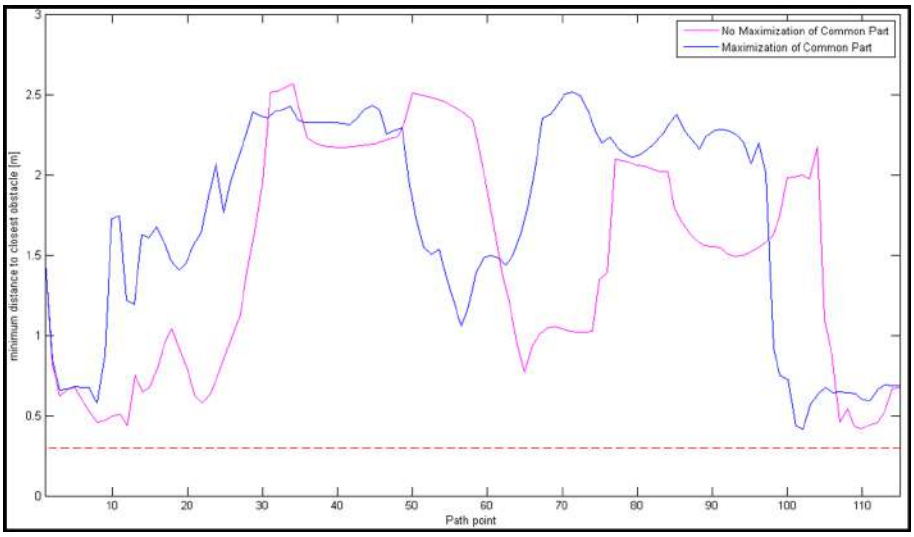

Figure 26: Comparison of the minimum distances to the closest obstacles using line guidance trajectories to port 13, with and without maximization of common part.

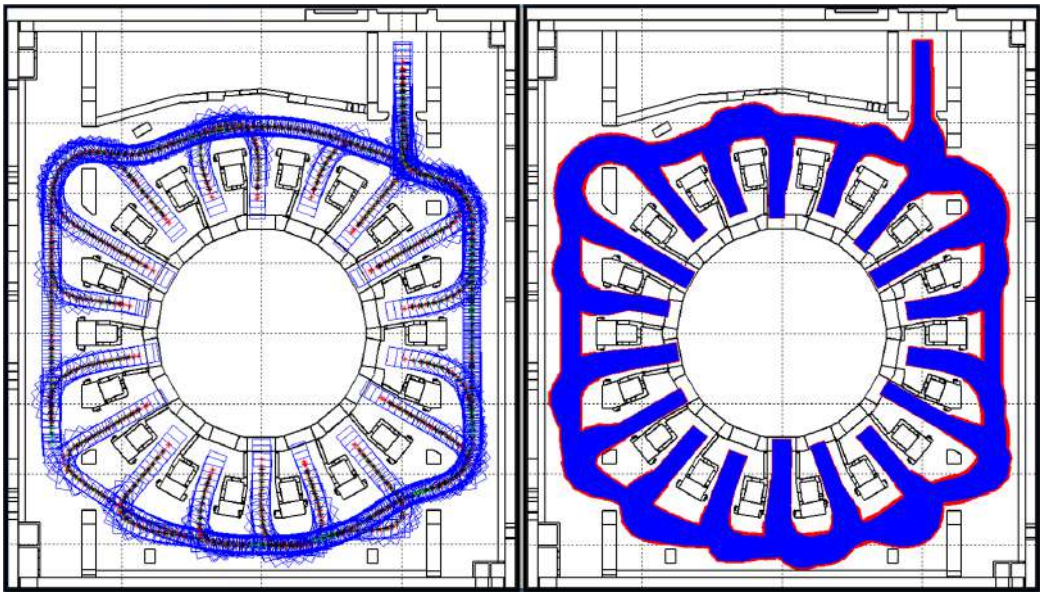

Figure 27: The optimized trajectories for all ports in level B1 of TB (left image) and the respective spanned area (right image).

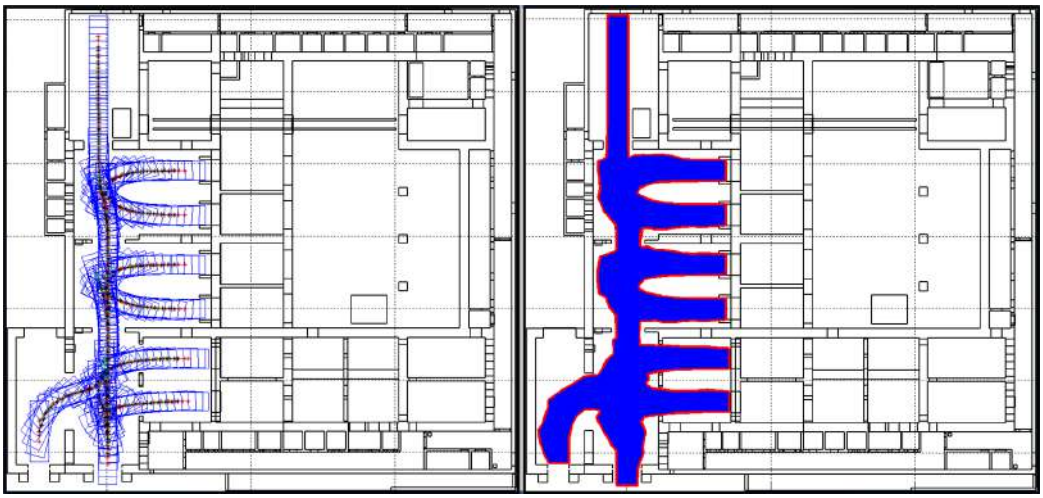

Figure 28: The optimized trajectories for all ports in level L1 of HCB (left image) and the respective spanned area (right image).

4. Conclusions and Future Work

This paper presented the trajectory optimization strategies developed for remote handling systems that will operate in ITER, for transporting heavy and highly activated in-vessel components between the Tokamak Building and the Hot Cell Building. Two main approaches were developed for trajectory optimization, providing smooth paths that maximize the clearance to obstacles, taking into account the features of rhombic like vehicles: line guidance (both wheels following the same path) and free roaming (different paths for each wheel). Whenever possible, the line guidance approach with or without maneuvers is adopted as the final solution. If not possible, the free roaming is selected. The trajectories were evaluated maximizing the common paths in the same level of each building. The maximized path is line guidance, since both wheels follows the same path. The branches to each port could also be line guidance or free roaming.

The two main approaches were implemented in a standalone application that receives the 3D CAD models of each level of the buildings, converts them into 2D models and, using the specifications of the missions and the models of the vehicles, returns the best trajectories, including a report of the most risky points of collision and the swept volume of the vehicle along the missions to CATIA V5R19 software. More than five hundred trajectories were evaluated, most of them using line guidance, some of them with 1 and few with 2 maneuvers. The most critical points are in the vicinity of the pillars and in the entrance to the lift of ports, where sometimes the free roaming is the only feasible solution. The main conclusions of trajectory optimization were provided to the ITER Organization by the Fusion For Energy and they were crucial to proceed with the construction of the Tokamak Building. For instance the doors aperture profiles (angle and orientation) were adjusted to reduce the risk of clashes.

The required trajectories were computed offline. However, the actual implementation can be reverted into a version to run in real time. The decision of selecting line guidance and free roaming is manually, as similar to the decision to include a maneuver and the respective point of maneuver. In the future, the decision of selecting line guidance or free roaming can be done based on the minimum distances to the obstacles, as the decision of including or not maneuvers. The decision of where to put a point of maneuver remains as an open issue. The line guidance approach is a deterministic process, while free roaming may converge to similar solutions, since the initialization

is random given the Rapidly-Exploring Random Tree component. The initialization of the line guidance approach is deterministic and based on the Constrained Delaunay Triangulation. The Fast Marching [23] is under study as a possible replacement for the initialization of the line guidance to speed up the entire process.

The velocity profile in the trajectory will be improved taking into account approaches with dynamics and the risk of huge vehicle in cluttered environments, which is the next instance of development and improvement of TES.

5. Acknowledgments

The work was supported by the grants F4E-2008-GRT-016 (MS-RH) and F4E-GRT-276-01 (MS-RH) funded by the European Joint Undertaking for ITER and the Development of Fusion for Energy (F4E) and by FCT in the frame of the Contract of Associate Laboratories of Instituto de Plasmas e Fusão Nuclear/IST (PEst-OE/SADG/LA0010/2011) and Laboratório de Robótica e Sistemas em Engenharia e Ciências/IST (PEst-OE/EEI/LA0009/2011). The views expressed in this publication are the sole responsibility of the authors. F4E is not liable for the use which might be made of the information in this publication.

References

[1] R. P. Feynman, R. B. Leighton and M. Sands, "The Feynman Lectures on Physics", Addison Wesley, vol. I, Sec. 9.6, 1963.

[2] P. E. Hart, N.J. Nilsson and B. Raphael, "A Formal Basis for the Heuristic Determination of Minimum Cost Paths", IEEE Transactions on Systems Science and Cybernetics, vol. 4, pp. 100 - 107, July 1968.

[3] T . Lozano-Pérez and M. A. Wesley, "An algorithm for planning collision-free paths among polyhedral obstacles", Communications of the ACM, vol. 22, pp. 560-570, New York, USA, 1979.

[4] J. F. Canny, "A Voronoi Method for the Piano-Movers Problem", Proceedings of IEEE International Conference on Robotics and Automation, pp. 530-535, USA, 1985.

[5] L. P. Chew, "Constrained Delaunay Triangulations", Proceedings of the Third Annual Symposium on Computational Geometry, pp. 215-222, Waterloo, Ontario, Canada, 1987.

[6] M. Kass, A. Witkin and D. Terzopoulos, "Snakes: active contour models", Int. Journal Computer Vision, vol. 1, No. 4, pp. 321-331, 1988.

[7] S. Quinlan and O. Khatib, "Elastic Bands: Connecting Path Planning and Control", Proceedings IEEE Conference Robotics and Automation, vol. 2, pp. 802-807, Atlanta, USA, 1993.

[8] F. Kang and S. Zhong-Ci, "Mathematical Theory of Elastic Structures", Science Press, China, 1995.

[9] L. E. Kavraki, P. Svestka, J.-C. Latombe and M. H. Overmars, "Probabilistic roadmaps for path planning in high-dimensional configuration spaces", IEEE Transactions on Robotics and Automation, vol. 12, pp. 566-580, 1996.

[10] M. I. Ribeiro, P. Lima, R. Aparcio and R. Ferreira, "Conceptual Study on Flexible Guidance and Navigation for ITER Remote Handling Transport Casks", Proceedings of the 17th IEEE/NPSS Symposium on Fusion Engineering, pp. 969-972, San Diego, USA, 1997.

[11] S. M. LaValle, "Rapidly-exploring random trees: A new tool for path planning", Computer Science Dept., Iowa State University, TR: 98-11.

[12] M. U. Ascher and L. R. Petzold, "Computer methods for ordinary differential equations and differential - algebraic equations", Society for Industrial and Applied Mathematics, 1998.

[13] J. J. Kuffner Jr and S. M. Lavalle, "RRT-Connect: An efficient approach to single-query path planning", in IEEE International Conference on Robotics and Automation, 2000.

[14] S. M. LaValle, J. J. Kuffner, "Rapidly-exploring random trees: Progress and prospects" In B. R. Donald, K. M. Lynch, and D. Rus., editors, Algorithmic and Computational Robotics: New Directions, pp. 293-308, A K Peters, Wellesley, MA, 2001.

[15] Wang, Danwei. "Trajectory Planning for a Four-Wheel-Steering Vehicle", Electronic Engineering, pp. 3320-3325, ISBN: 0780364759, 2001.

[16] F. P. Beer, E. R. Johnston and J. T. DeWolf, "Mechanics of Materials", McGraw Hill, 2002.

[17] E. Hairer, C. Lubich and G. Wanner, "Geometric numerical integration illustrated by the Stormer Verlet method", Acta Numerica, vol. 12, pp. 399-450, 2003.

[18] O. Castilho; L. Trujilo. "Multiple Objective Optimization Genetic Algorithms For Path Planning In Autonomous Mobile Robots". International Journal of Computers, Systems and Signal, vol. 6, No.1, pp. 648-63, 2005.

[19] Qing Li; Xinhai Tong; Sijiang Xie; Yingchun Zhang, "Optimum Path Planning for Mobile Robots Based on a Hybrid Genetic Algorithm", Hybrid Intelligent Systems, 2006. HIS'06. Sixth International Conference, pp. 53, 2006.

[20] K.R. Schultz, "Why Fusion? A discussion of energy alternatives", Control Systems Magazine, IEEE, vol. 26, issue:2, pp. 32-34, April 2006.

[21] Hans-Wilhelm Schiffe, "World Energy Congress – Energy policy scenarios to 2050", vol. 36, Issue 7, pp. 2464-2470, July 2008.

[22] C. Gutiérrez, C. Damiani, M. Irving, J-P. Friconneau, A. Tesini, M.I. Ribeiro and A. Vale, "ITER Transfer Cask System: status of design, issues and future developments", Proceedings of the 9th International Symposium on Fusion Nuclear Energy, China, 2009.

[23] S. Garrido, L. Moreno, D. Blanco, F .Martin. "Smooth Path Planning for non-holonomic robots using Voronoi Fast Marching", 5th IEEE International Conference on Mechatronics , pp. 1-6, Mlaga. Spain, ISBN: 9781424441945, April 2009.

[24] Gregory Dudek and Michael Jenkin, "Computational Principles of Mobile Robotics", Cambridge University Press, ISBN: 9780521692120, (2 edition) 2010.

[25] D. Fonte, F. Valente, A. Vale and I. Ribeiro, "A Motion Planning Methodology for Rhombic-like Vehicles for ITER Remote Handling Operations", Proceedings of the 7th IFAC Symposium on Intelligent Autonomous Vehicles, Lecce, Italy, 2010.

[26] J.M. Martn, D. Lpez, F. Gmez-Bravo, A. Blanco. "Application of multicriteria decision-making techniques to manoeuvre planning in nonholonomic robots". Expert Systems with Applications, vol. 37, No.5, pp. 3962-3976, 2010.

[27] P. Ruibanys, C. Reig, E. Gazeau, J. Marmie and N. Etchegoin, "Definition, Development and Operation of a Comprehensive Virtual Model of the ITER Buildings, ATS and TCS", 26th Symposium on Fusion Technology, Porto, 2010.

[28] Optimized Trajectories of the Transfer Cask System in ITER. Filipe Valente, Alberto Vale, Daniel Fonte, Isabel Ribeiro. Fusion Engineering and Design, 86, pp. 1967-1970, 2011.

[29] D. Fonte, F. Valente, A. Vale, I. Ribeiro, "Path Optimization of Rhombic-Like Vehicles: An Approach Based on Rigid Body Dynamic", Proceedings of the 15th IEEE International Conference on Advanced Robotics, pp. 106-111, Tallinn, Estonia, June 20-23, 2011.

[30] United Nations Population Fund – State of World Population 2011 – People and Possibilities in a World of 7 Billion, ISBN: 9780897149907, 2011.